



**HAL**  
open science

## Rate constants for the $N(2D) + C_2H_2$ reaction over the 50–296 K temperature range

Dianailys Nuñez-Reyes, Jean-Christophe Loison, Kevin Hickson, Michel Dobrijevic

► **To cite this version:**

Dianailys Nuñez-Reyes, Jean-Christophe Loison, Kevin Hickson, Michel Dobrijevic. Rate constants for the  $N(2D) + C_2H_2$  reaction over the 50–296 K temperature range. *Physical Chemistry Chemical Physics*, 2019, 21 (40), pp.22230-22237. 10.1039/C9CP04170B . hal-02322145

**HAL Id: hal-02322145**

**<https://hal.science/hal-02322145>**

Submitted on 11 Jan 2021

**HAL** is a multi-disciplinary open access archive for the deposit and dissemination of scientific research documents, whether they are published or not. The documents may come from teaching and research institutions in France or abroad, or from public or private research centers.

L'archive ouverte pluridisciplinaire **HAL**, est destinée au dépôt et à la diffusion de documents scientifiques de niveau recherche, publiés ou non, émanant des établissements d'enseignement et de recherche français ou étrangers, des laboratoires publics ou privés.

# Rate Constants for the $N(^2D) + C_2H_2$ Reaction over the 50 – 296 K Temperature Range.

Dianailys Nuñez-Reyes,<sup>a,b</sup> Jean-Christophe Loison,<sup>a,b</sup> Kevin M. Hickson,<sup>a,b,\*</sup> and Michel

Dobrijevic<sup>c</sup>

<sup>a</sup>*Université de Bordeaux, Institut des Sciences Moléculaires, UMR 5255, F-33400 Talence, France*

<sup>b</sup>*CNRS, Institut des Sciences Moléculaires, UMR 5255, F-33400 Talence, France*

<sup>c</sup>*Laboratoire d'Astrophysique de Bordeaux, Université de Bordeaux, CNRS, B18N, allée Geoffroy Saint-Hilaire, F-33615 Pessac, France*

*corresponding author e-mail: kevin.hickson@u-bordeaux.fr*

## Abstract

The reactions of metastable atomic nitrogen  $N(^2D)$  are important processes in the gas-phase chemistry of several planetary atmospheres. Here we present a combined experimental and theoretical investigation of the  $N(^2D) +$  acetylene reaction due to its potential significance for the photochemistry of Titan's atmosphere. Experimentally, a continuous supersonic flow reactor was used to study this reaction over the 50-296 K temperature range employing pulsed laser photolysis and vacuum ultraviolet laser induced fluorescence to produce and detect  $N(^2D)$  atoms respectively. The measured rate constants are substantially larger than those obtained in earlier work and remain constant as a function of temperature. Moreover, these results are supported by new electronic structure calculations which indicate that this process is likely to be barrierless. The impact of the new rate constants on Titan's atmospheric chemistry is tested through simulations using a 1D coupled ion-neutral photochemical model.

## 1 Introduction

Atomic nitrogen is present in a variety of different environments, contributing to the complex chemistry of the interstellar medium, planetary atmospheres and combustion processes. Atomic nitrogen in its ground electronic state,  $N(^4S)$ , is significantly less reactive with neutral coreagents at low and intermediate temperatures than its oxygen and carbon counterparts ( $O(^3P)$  and  $C(^3P)$  respectively), essentially only reacting with radical species.<sup>1-5</sup> In contrast, atomic nitrogen in its first excited state,  $N(^2D)$ , has already been shown through kinetic studies to react much more rapidly with a range of closed shell molecules including saturated<sup>6-10</sup> and unsaturated<sup>6, 7, 11, 12</sup> hydrocarbons alike. This could have important consequences for the

chemistry of planetary atmospheres with large molecular nitrogen mixing ratios such as the Earth or Saturn's moon Titan. In Earth's upper atmosphere,  $N_2$  photolysis in the vacuum ultraviolet (VUV) wavelength range produces important quantities of  $N(^4S)$ ,  $N(^2D)$  and higher excited states such as  $N(^2P)^{13}$  which is mostly unreactive. As non-reactive quenching of  $N(^2D)$  by  $N_2$  is slow, in the case of the Earth,  $N(^2D)$  is mostly removed through its reaction with atmospheric  $O_2$  to produce  $NO$ ; a molecule whose concentration is ultimately limited by its reactions with  $N(^4S)$  and  $N(^2D)$ .<sup>14, 15</sup> In Titan's atmosphere, current photochemical models predict that  $N(^2D)$  should react with the most abundant stable molecules including  $CH_4$ ,  $C_2H_6$ ,  $C_2H_4$  and  $C_2H_2$  providing several potentially important pathways for the formation of nitrogen-bearing hydrocarbon species. While there are several previous dynamical investigations of these reactions, providing detailed information on the preferred product channels,<sup>16-21</sup> kinetic studies are sparse, particularly as a function of temperature. Nunez-Reyez et al.<sup>22</sup> recently studied the kinetics of the  $N(^2D) + CH_4$ ,  $C_2H_6$  and  $C_3H_8$  reactions over the 75–296 K temperature range. The new results for the  $N(^2D) + CH_4$  reaction were in good agreement with earlier work over the 223-293 K range,<sup>6-8, 10</sup> thereby validating the rate constants recommended by Herron.<sup>23</sup> In contrast, the only previous measurements of the rate constants for the  $N(^2D) + C_2H_6$  and  $C_3H_8$  reactions had been performed at room temperature, so that photochemical models adopted the room temperature values to describe the reactivity at temperatures relevant to Titan's atmosphere. Nunez-Reyez et al.<sup>22</sup> clearly showed that the reactivity of both of these processes decreases as the temperature falls, making them negligibly important to the overall photochemistry. The kinetics of the reaction between  $N(^2D)$  and  $C_2H_2$  has already been studied at room temperature by Fell et al.<sup>7</sup> and over the 223-293 K range by Takayanagi et al.<sup>12</sup> The rate constants measured by Takayanagi et al.<sup>12</sup> were seen to fall at lower temperature; an observation which was supported by quantum-chemical calculations that predicted the likely presence of a small activation barrier for this reaction. Later crossed molecular beam measurements by Balucani et al.<sup>20</sup> clearly demonstrated that this reaction leads almost exclusively to  $H + HCCN$  as products, making it the major source of  $HCCN$  radicals in Titan's atmosphere. Indeed, a large part of the rich nitrile chemistry in Titan's upper atmosphere is thought to originate from reactions of the  $HCCN$  radical. In particular, current photochemical models consider that the reaction between  $H$  and  $HCCN$  is an efficient pathway for the formation of  $CCN$  radicals which go on to react with  $C_2H_2$  and  $C_2H_4$  at high altitude through an addition-elimination mechanism, producing longer carbon chain nitriles such as  $CH_3C_3N$ .<sup>24</sup>

In this work, we report new measurements of the rate constants for the  $N(^2D) + C_2H_2$  reaction over the 50-296 K temperature range using the CRESU (cinétique de réaction en

écoulement supersonique uniforme) technique. Here, a chemical reaction was used to produce  $N(^2D)$  atoms, which were followed directly by on-resonance pulsed laser induced fluorescence. In parallel, we report new electronic structure calculations, which were performed to derive the relevant stationary points along the reaction coordinate for a more complete understanding of the experimental results. The experimental and theoretical methods are presented in sections 2 and 3 respectively. The experimental results presented in section 4 are discussed in the context of the present and previous experimental and theoretical work in section 5. The effects of the new rate constants on a photochemical model of Titan’s atmosphere are also described in Section 5. Our conclusions are presented in section 6.

## 2 Experimental methods

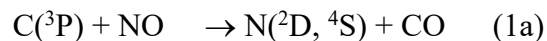
The measurements reported here were performed using a supersonic flow (Laval nozzle) apparatus, which has been described in previous work.<sup>25-27</sup> Later studies report the various modifications applied to the original experiment to allow narrowband tunable vacuum ultraviolet radiation to be generated for the detection of several atomic species in their ground and excited electronic states ( $C(^3P)$ ,<sup>28-30</sup>  $H(^2S)$ <sup>28, 30-38</sup> and  $D(^2S)$ ,<sup>30, 39</sup>  $O(^1D)$ <sup>35, 38, 40-44</sup> and  $N(^2D)$ <sup>15, 22</sup>). Experiments were performed using argon and nitrogen based Laval nozzles during the present work as  $N(^2D)$  atoms are only slowly quenched by both of these gases.<sup>45, 46</sup> The detailed characteristics of the various Laval nozzles used in this study are listed in Table 1.

**Table 1** Supersonic flow characteristics

Mach number	$1.83 \pm 0.02^a$	$1.99 \pm 0.03$	$2.97 \pm 0.06$	$3.85 \pm 0.05$
Carrier gas	$N_2$	Ar	Ar	Ar
Density ( $\times 10^{16} \text{ cm}^{-3}$ )	$9.4 \pm 0.2$	$12.6 \pm 0.3$	$14.7 \pm 0.6$	$25.9 \pm 0.9$
Impact pressure (Torr)	$8.2 \pm 0.1$	$10.5 \pm 0.2$	$15.3 \pm 0.5$	$29.6 \pm 1.0$
Stagnation pressure (Torr)	10.3	13.9	34.9	113.2
Temperature (K)	$177 \pm 2$	$127 \pm 2$	$75 \pm 2$	$50 \pm 1$
Mean flow velocity ( $\text{ms}^{-1}$ )	$496 \pm 4$	$419 \pm 3$	$479 \pm 3$	$505 \pm 1$
Chamber pressure (Torr)	1.4	1.5	1.2	1.4

<sup>a</sup> The errors on the Mach number, density, temperature and mean flow velocity ( $1\sigma$ ) are calculated from separate measurements of the impact pressure as a function of distance from the Laval nozzle using a Pitot tube and the stagnation pressure within the reservoir.

The room temperature measurements described here were performed by removing the nozzle and by significantly reducing the flow velocity in the chamber, effectively employing the reactor as a slow-flow flash photolysis apparatus. During this work, ground state C(<sup>3</sup>P) atoms were used as the source of N(<sup>2</sup>D) atoms, through the chemical reaction



as previously described by Nunez-Reyes & Hickson,<sup>15</sup> and Nunez-Reyes et al.<sup>22</sup> Here, C(<sup>3</sup>P) is generated by the pulsed multiphoton dissociation of tetrabromomethane (CBr<sub>4</sub>) at 266 nm. By aligning the photolysis laser beam along the axis of the reactor, these radicals were produced with a uniform concentration along the entire length of the supersonic flow. Although the exact branching ratio towards N(<sup>2</sup>D) of reaction (1) is unknown (only the total atomic nitrogen production N(<sup>2</sup>D) + N(<sup>4</sup>S) has been estimated at 298 K<sup>47</sup>), its yield has already been shown to be large enough to perform kinetic studies of N(<sup>2</sup>D) reactions over the 50-296 K range.<sup>15</sup> CBr<sub>4</sub> vapour with an estimated concentration of less than 3.2 × 10<sup>13</sup> cm<sup>-3</sup> was carried into the reactor by diverting a small part of the carrier gas flow into a vessel containing solid CBr<sub>4</sub> maintained at a fixed pressure and temperature. In common with previous work, N(<sup>2</sup>D) atoms were detected by pulsed laser induced fluorescence in the vacuum ultraviolet wavelength range (VUV LIF). The procedure for generating tunable VUV radiation at 116.745 nm has already been described elsewhere.<sup>15</sup> The VUV radiation was directed into the reactor at right angles to both the supersonic flow and the detector through a 75 cm sidearm containing baffles; a configuration which represented the optimal geometry to minimize the detection of scattered VUV and residual UV light. As reagent C<sub>2</sub>H<sub>2</sub> has a large absorption cross section of approximately (3-4) × 10<sup>-17</sup> cm<sup>2</sup> at this wavelength at room temperature, the sidearm was flushed with N<sub>2</sub> or Ar to maximize the transmission of the VUV probe laser.

Resonant fluorescence from unreacted N(<sup>2</sup>D) atoms within the supersonic flow was detected by a solar-blind photomultiplier tube (PMT) which was protected from reactive gases by a lithium fluoride (LiF) window. A LiF lens was placed between the LiF window and the PMT to focus the emitted light onto the PMT photocathode, while this region was also evacuated to prevent atmospheric absorption losses. The PMT output signal was amplified before signal processing and integration by a boxcar system. Unfortunately, as the amplifier was saturated for 15 microseconds following the intense photolysis pulse, no VUV LIF signals could be recorded during this time period. The lasers, boxcar and oscilloscope used to monitor the fluorescence signal throughout the experiments were synchronized by a digital delay generator. 30 laser shots

were recorded and averaged at each time point with each kinetic profile consisting of at least 70 time points. The baseline level was set by recording several points at negative time delays where the probe laser fired before the photolysis laser. Gases (Linde Ar 99.999%, Xe 99.999%, C<sub>2</sub>H<sub>2</sub> 99.6%, Air Liquide N<sub>2</sub> 99.999%, NO 99.9%) were used without further purification directly from the cylinders. Calibrated mass-flow controllers were used to regulate the gas flows into the reactor.

### 3 Theoretical methods

To rationalize the experimental results, with the aim of understanding the discrepancies between the present and previous measurements and theoretical calculations, we have performed a new theoretical study of the N(<sup>2</sup>D) + C<sub>2</sub>H<sub>2</sub> reaction. In the N(<sup>2</sup>D) + C<sub>2</sub>H<sub>2</sub> system, five doublet potential energy curves (<sup>2</sup>A<sub>1</sub>, two <sup>2</sup>A<sub>2</sub>, <sup>2</sup>B<sub>1</sub> and <sup>2</sup>B<sub>2</sub>) correlate with these reagents in C<sub>2v</sub> symmetry when N approaches perpendicularly to the C≡C bond of acetylene (two <sup>2</sup>A' and three <sup>2</sup>A'' states in C<sub>s</sub> symmetry when N approaches toward the C≡C bond of acetylene at other angles). The electronic state of N(<sup>2</sup>D) is fivefold degenerate in the absence of spin-orbit interactions. As shown by Takayanagi et al.,<sup>12, 48</sup> it is crucial to employ a method that allows the multiconfigurational aspect of N(<sup>2</sup>D) reactivity to be taken into account. Consequently, we use Complete Active Space Self-Consistent field (CASSCF) calculations using 11 active orbitals and 12 active electrons. With the resulting molecular orbitals, the ic-MRCI-F12 energies (internally contracted MultiReference Configuration Interaction) were calculated using the MOLPRO suite of programs with an augmented triple zeta atomic basis set, aug-cc-VTZ. The geometry was optimized at the MCSCF level for each distance between N and the center of mass of acetylene. We compare our results with previous calculations<sup>12, 48</sup> made to demonstrate the critical nature of the calculation level.

### 4 Experimental Results

All the kinetic experiments performed here applied the pseudo-first-order approximation, where excess concentrations of both NO and C<sub>2</sub>H<sub>2</sub> were used (with respect to minor reagents C(<sup>3</sup>P) and N(<sup>2</sup>D)). Under these conditions, the temporal evolution of N(<sup>2</sup>D) atoms followed through their VUV LIF signal,  $I_{N(^2D)}$  is described by the following expression

$$I_{N(^2D)} = A(\exp(-k'_a t) - \exp(-k'_b t)) \quad (2)$$

where A is a constant,  $k'_a$  is the pseudo-first-order rate constant for N(<sup>2</sup>D) removal,  $k'_b$  is the pseudo-first-order rate constant for N(<sup>2</sup>D) production and  $t$  is time. The term  $k'_a$  comprises

several contributions including the pseudo-first-order losses of  $N(^2D)$  with excess coreagents NO ( $k_{N(^2D)+NO}[NO]$ ) and  $C_2H_2$  ( $k_{N(^2D)+C_2H_2}[C_2H_2]$ ), precursor molecule  $CBr_4$  ( $k_{N(^2D)+CBr_4}[CBr_4]$ ) and diffusion ( $k_{N(^2D),diff}$ ). As  $C(^3P)$  atoms react with both NO and  $C_2H_2$ ,  $k'_b = k_{C(^3P)+NO}[NO] + k_{C(^3P)+C_2H_2}[C_2H_2] + k_{C(^3P),diff}$ . Nevertheless, as the first 15  $\mu s$  of the  $N(^2D)$  temporal profiles could not be exploited due to signal saturation issues, a function of the form

$$I_{N(^2D)} = A \exp(-k'_a t) \quad (3)$$

was used instead to describe the  $N(^2D)$  signal as a function of time, fitting only to the decaying part of the temporal profiles. Figure 1 shows two profiles of the  $N(^2D)$  fluorescence intensity as a function of time recorded at 50 K in the presence and absence of  $C_2H_2$ .

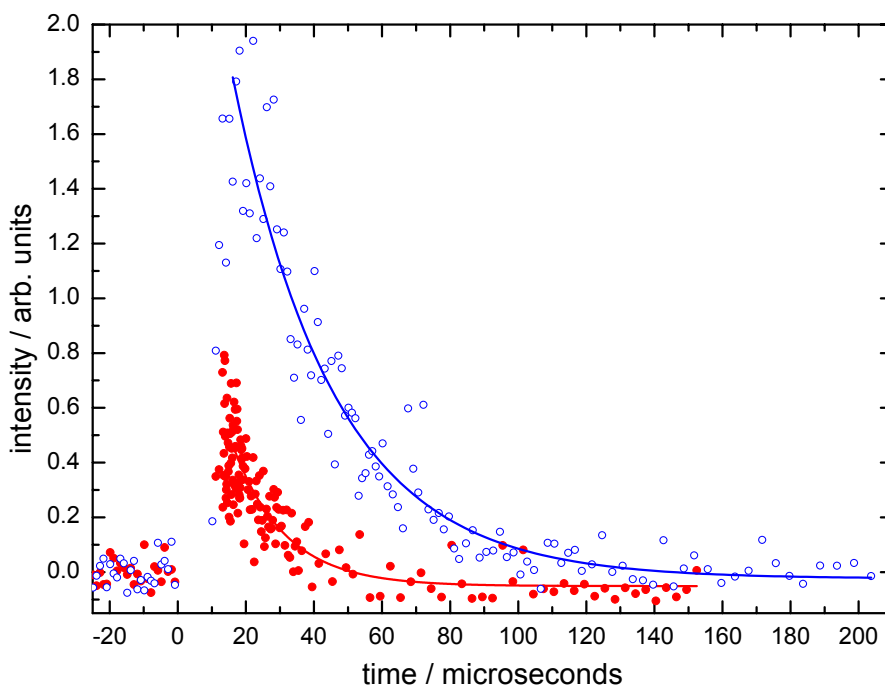
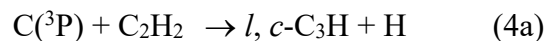


**Figure 1**  $I_{N(^2D)}$  as a function of time recorded at 50 K. (Open blue circles) without  $C_2H_2$ ; (solid red circles)  $[C_2H_2] = 2.7 \times 10^{14} \text{ cm}^{-3}$ .  $[NO] = 3.1 \times 10^{14} \text{ cm}^{-3}$  for this series of experiments. Solid red and blue lines represent exponential fits to the individual datasets using expression (3).

### Effects of the competing $C(^3P) + C_2H_2$ reaction

As C(<sup>3</sup>P) atoms are unreactive with saturated hydrocarbons, Nunez-Reyes et al.<sup>22</sup> were able to investigate the reactions of N(<sup>2</sup>D) with CH<sub>4</sub>, C<sub>2</sub>H<sub>6</sub> and C<sub>3</sub>H<sub>8</sub> without additional interferences from these reagents. In the present case, C(<sup>3</sup>P) atoms are known to react rapidly with acetylene through reaction (4);<sup>34, 49, 50</sup>



a process which is in direct competition with reaction (1) in the supersonic flow leading to a corresponding decrease in the N(<sup>2</sup>D) production efficiency. Consequently, the range of excess C<sub>2</sub>H<sub>2</sub> and NO concentrations used in the experiments had to be carefully chosen so that enough N(<sup>2</sup>D) atoms could be produced through reaction (1) (where [NO] is constant for any series of experiments) to be able to follow the progress of the N(<sup>2</sup>D) + C<sub>2</sub>H<sub>2</sub> reaction. It can be clearly seen from Figure 1 that at high [C<sub>2</sub>H<sub>2</sub>], fewer N(<sup>2</sup>D) atoms are produced compared to experiments conducted without C<sub>2</sub>H<sub>2</sub>, as reaction (4) dominates the loss of C(<sup>3</sup>P) atoms. The peak intensity of the N(<sup>2</sup>D) VUV LIF signal is also shifted to shorter times due to the faster loss of C(<sup>3</sup>P) atoms. Consequently, due to the aforementioned signal saturation issues, the maximum [C<sub>2</sub>H<sub>2</sub>] was chosen to provide peak N(<sup>2</sup>D) intensities at times greater than 15 μs. At low [C<sub>2</sub>H<sub>2</sub>], peak N(<sup>2</sup>D) signals were larger and shifted to longer times. In this instance, care had to be taken to fit to only the part of the kinetic profiles where C(<sup>3</sup>P) atom loss (and N(<sup>2</sup>D) production) was finished. Interestingly, in our previous work on the kinetics of the N(<sup>2</sup>D) + C<sub>x</sub>H<sub>2x+2</sub> reactions, a large number of the early time points (where the N(<sup>2</sup>D) VUV LIF signal is highest) could not be exploited due to the slow nature of N(<sup>2</sup>D) atom production. In the present study, although the peak signal levels were lower, many more early time points could be exploited due to the more rapid removal of C(<sup>3</sup>P). Moreover, as the rate constant for the N(<sup>2</sup>D) + C<sub>2</sub>H<sub>2</sub> reaction is significantly larger than those of the N(<sup>2</sup>D) + C<sub>x</sub>H<sub>2x+2</sub> reactions, much lower concentrations of coreagent C<sub>2</sub>H<sub>2</sub> could be used, leading to lower attenuation levels of the VUV excitation source and fluorescence emission. Taking these two effects into consideration meant that the signal intensities were actually comparable to those obtained in our previous work on N(<sup>2</sup>D) + C<sub>x</sub>H<sub>2x+2</sub> reactions.<sup>22</sup> In addition to the various effects of reaction (4) on the N(<sup>2</sup>D) signal levels, we also need to consider potential interferences from secondary chemistry. Several of the reactions that could interfere with our measurements have already been discussed by Nuñez-Reyes & Hickson<sup>15</sup> and by Nuñez-Reyes et al.<sup>22</sup> Here, we also need to consider the reactions of the products of reaction (4) on the overall chemistry, and in particular we need to consider the possibilities for secondary N(<sup>2</sup>D) atom production as these kinetic studies follow N(<sup>2</sup>D) directly.

The  $C_3$  radical has a singlet ground state and is unreactive with most stable molecules so that the reactions of  $C_3$  with  $C_2H_2$  and  $NO$  are both slow at room temperature<sup>51, 52</sup> and should therefore play no role in the overall chemistry. Similarly, according to Benedikt et al.<sup>53</sup> the reaction of  $C_3H$  with  $C_2H_2$  is also very slow. Although theoretical studies by Xie et al.<sup>54</sup> have shown that the *l,c*- $C_3H + NO$  reactions should occur without a barrier, the products are thought to be  $HCCN$  and  $CO$ . In turn, Adamson et al.<sup>55</sup> showed that  $HCCN$  can react with  $NO$  but without leading to  $N(^2D)$  formation while the  $HCCN + C_2H_2$  reaction was seen not to occur. In this respect, it seems unlikely that secondary reactions involving product species would significantly alter the measured kinetic profiles.

Several decays of the type displayed in Figure 1 were recorded at each  $[C_2H_2]$ , while experiments were performed with at least 9 different  $[C_2H_2]$  at each temperature.  $[NO]$  was maintained at a fixed value for any individual series of experiments so that changes in the  $N(^2D)$  atom decay rate were only due to the variation of  $[C_2H_2]$ . Second-order rate constants were obtained from the slope of plots of the derived pseudo-first-order rate constant versus  $[C_2H_2]$ , through weighted linear least-squares fits to the data. Figure 2 shows two such second-order plots recorded at 50 K (solid blue squares) and 296 K (solid red squares).

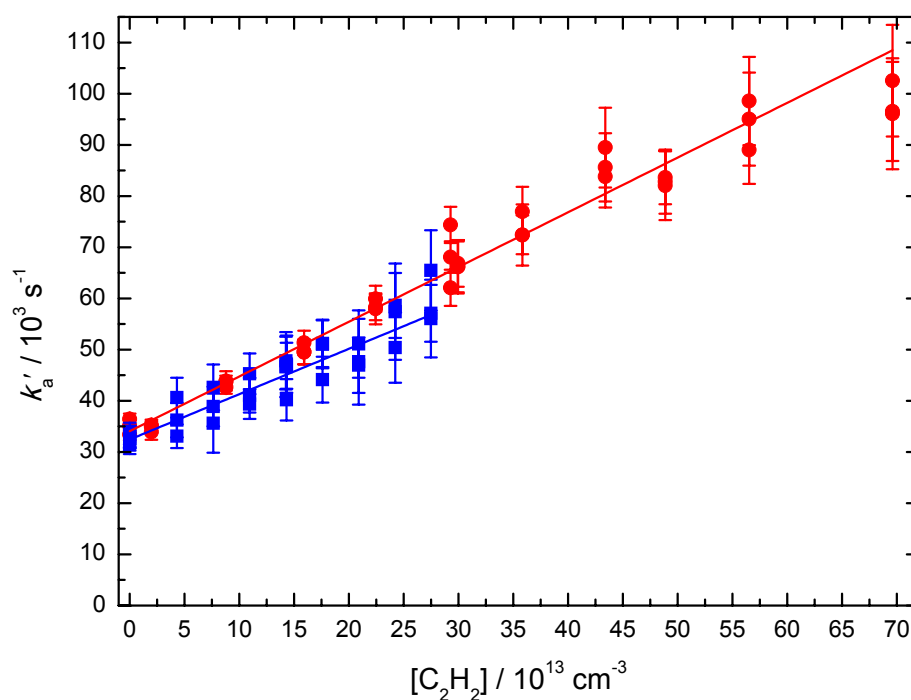


**Figure 2** Measured pseudo-first-order rate constant  $k'_a$  as a function of  $[C_2H_2]$ . (Red solid circles) 296 K; (blue solid squares) 50 K. Solid blue and red lines represent weighted linear least-squares fits to the data. The error bars on individual data points, shown at the level of a single standard deviation, are derived from exponential fits to temporal profiles such as those displayed in Figure 1 using expression (3).

The measured second-order rate constants are displayed as a function of temperature in Figure 3 alongside earlier measurements over the 223-298 K range. These values are also summarized in Table 2 with other relevant information.

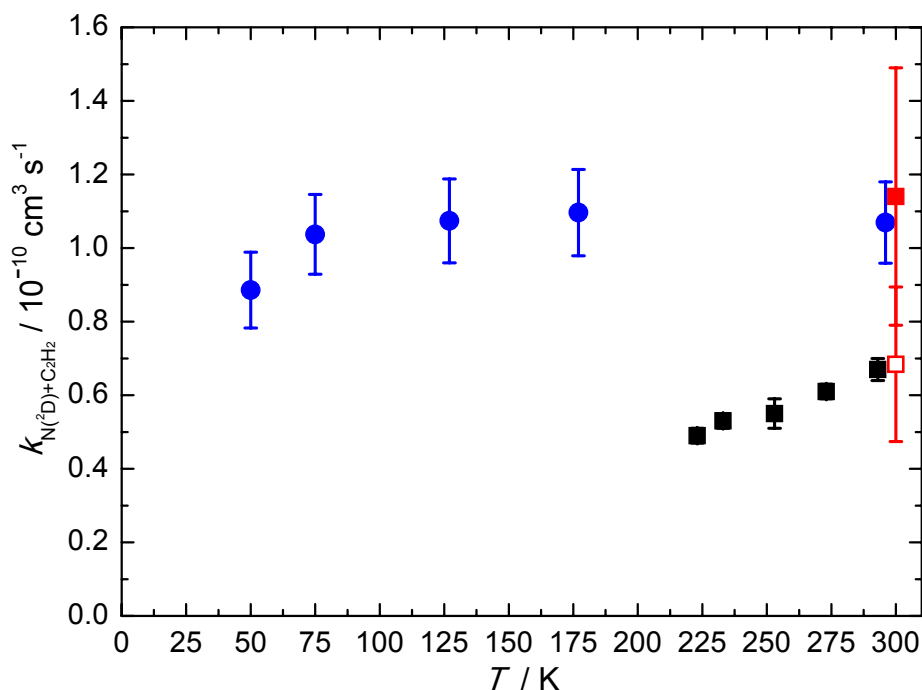


**Figure 3** Temperature dependence of the rate constant for the  $N(^2D) + C_2H_2$  reaction. (Red solid square) Fell et al. uncorrected;<sup>7</sup> (Red open square) Fell et al. corrected;<sup>23</sup> (black solid squares) Takayanagi et al.;<sup>12</sup> (blue solid circles) this work. Error bars on the present values represent the statistical ( $1\sigma$ ) and systematic uncertainties (estimated to be 10 %).

**Table 2** Temperature dependent rate constants for the  $N(^2D) + C_2H_2$  reaction

T / K	$N^b$	$[NO] / 10^{14} \text{ cm}^{-3}$	$[C_2H_2] / 10^{14} \text{ cm}^{-3}$	$k_{N(^2D)+C_2H_2} / 10^{-11} \text{ cm}^3 \text{ s}^{-1}$
-------	-------	----------------------------------	--------------------------------------	--

296	36	4.3	0 - 7.0	$(10.7 \pm 1.1)^c$
$177 \pm 2^a$	36	2.7	0 - 4.4	$(11.0 \pm 1.2)$
$127 \pm 2$	50	3.1	0 - 5.4	$(10.7 \pm 1.1)$
$75 \pm 2$	36	2.7	0 - 2.5	$(10.4 \pm 1.1)$
$50 \pm 1$	32	3.1	0 - 2.7	$(8.9 \pm 1.0)$

<sup>a</sup>Uncertainties on the calculated temperatures represent the statistical ( $1\sigma$ ) errors obtained from Pitot tube measurements of the impact pressure. <sup>b</sup>Number of individual measurements.

<sup>c</sup>Uncertainties on the measured rate constants represent the combined statistical ( $1\sigma$ ) and estimated systematic (10%) errors.

## 5 Discussion and Astrophysical Implications

There are two previous kinetic studies of the  $N(^2D) + C_2H_2$  reaction. Fell et al.<sup>7</sup> used the microwave discharge of  $N_2$  in helium to produce  $N(^2D)$  atoms in their fast-flow reactor study.  $N(^2D)$  atoms were followed directly by electron spin resonance spectroscopy. They determined rate constants for a range of deactivation processes involving  $N(^2D)$ , including the  $N(^2D) + C_2H_2$  reaction, deriving a rate constant of  $(11.4 \pm 3.5) \times 10^{-11} \text{ cm}^3 \text{ s}^{-1}$  at 298 K; a value that is in excellent agreement with the one measured during the present investigation of  $(10.7 \pm 1.1) \times 10^{-11} \text{ cm}^3 \text{ s}^{-1}$ . Following Herron,<sup>23</sup> a correction factor of 0.6 is typically applied to the Fell et al.<sup>7</sup> value yielding a rate constant of  $(6.8 \pm 2.1) \times 10^{-11} \text{ cm}^3 \text{ s}^{-1}$ . The value of this corrective factor represents the typical observed differences between the measured values of Fell et al.<sup>7</sup> and the results of other groups who have investigated the same  $N(^2D)$  reactions. Nevertheless, the final values reported by Fell et al.<sup>7</sup> themselves are already subject to an estimated correction factor of 1.3 due to possible intermediate behavior between plug flow and laminar flow in their reactor. Moreover, these authors also state that for certain fast reactions ( $N(^2D) + C_2H_2$  being among these processes) they were required to use such low coreagent concentrations that the pseudo-first-order approximation might no longer be valid (the coreagent concentration may have varied as a function of distance along the reactor). In this respect, the use of a unique arbitrary multiplicative factor to correct the results obtained by Fell et al. seems inappropriate. In the only other study of the  $N(^2D) + C_2H_2$  reaction, Takayanagi et al.<sup>12</sup> measured rate constants for this process over the 223-293 K temperature range. Experiments were conducted in a steel vessel containing a mixture of  $N_2$ ,  $C_2H_2$  and He maintained near atmospheric pressure (700

Torr) which was irradiated by a pulsed electron beam to generate  $N(^2D)$  atoms. The decay of  $N(^2D)$  was followed by resonance absorption spectroscopy at 149 nm using a CW resonance lamp coupled with a VUV monochromator. Although this allowed Takayanagi and coworkers to follow  $N(^2D)$  atoms directly, the resolution was not sufficiently high to discriminate between the three atomic lines generated by transitions between the fine structure levels of the upper and lower electronic states. The measured rate constants of Takayanagi et al.<sup>12</sup> were seen to decrease slightly with decreasing temperature from  $(6.7 \pm 0.3) \times 10^{-11} \text{ cm}^3 \text{ s}^{-1}$  at 293 K to  $(4.9 \pm 0.2) \times 10^{-11} \text{ cm}^3 \text{ s}^{-1}$  at 223 K. These values are significantly lower than those derived in the present work and show a clear negative temperature dependence, with an Arrhenius fit to these earlier data yielding an activation energy  $E_a = 2 \text{ kJ mol}^{-1}$ . If we extrapolate these results to temperatures representative of Titan's upper atmosphere (170 K), we obtain a rate constant of  $3.3 \times 10^{-11} \text{ cm}^3 \text{ s}^{-1}$ ; more than three times lower than the present experimental results which are essentially temperature independent over the 50 - 296 K range considering the experimental error bars. The experimental results of Takayanagi et al.<sup>12</sup> were rationalized in the context of conventional statistical rate theory based on ab initio calculations of the intermediates and transition states of the relevant  $^2B_1$  doublet potential energy surface of the  $N(^2D) + C_2H_2$  reaction (the other four states which correlate with  $N(^2D) + C_2H_2$  were all found to be repulsive). In contrast to the experimental results, these calculations predicted a significant activation barrier (+ 12  $\text{kJ mol}^{-1}$  for the initial addition of  $N(^2D)$  to the  $C\equiv C$  bond in acetylene at the PMP4(full,SDTQ)/cc-pVTZ) level of theory using CASSCF geometry, leading to theoretical rate constants three or four orders of magnitude too low compared to the experimental ones. Indeed, it was only possible to reconcile the differences between the theoretical and experimental rate constants by lowering the barrier height to 0  $\text{kJ mol}^{-1}$  and by assuming fast nonadiabatic transitions between the attractive  $^2B_1$  state and the other four repulsive doublet states, effectively increasing the electronic partition function for this process from 0.2 to 1. In later work,<sup>48</sup> single point ab initio calculations were performed along the CASSCF intrinsic reaction coordinate path using a better level of theory (MRCI/cc-pVTZ) to more accurately obtain the barrier height. However, the results of variational transition state theory calculations using this classical barrier height (1.7  $\text{kJ mol}^{-1}$ ) were still unable to reproduce the experimental values. Only when the classical barrier height was lowered in the range 0.2-0.7  $\text{kJ mol}^{-1}$  using an electronic partition function of  $\sim 0.7$  did the calculated rate constants match the experimental ones. Crossed molecular beam experiments conducted by Balucani et al.<sup>20</sup> have since confirmed

the likelihood of a lower value for this barrier due to the observation of products at a collision energy of 13 kJ mol<sup>-1</sup>.

The previous theoretical calculations of Takayanagi et al.<sup>12, 48</sup> clearly demonstrate the importance of the method used to calculate the potential energy along the reaction coordinate for N(<sup>2</sup>D) attack on acetylene. While a barrier height of 21.8 kJ/mol was obtained at the CASSCF(7,7) level (7 active orbitals and 7 active electrons) with a VDZ basis, this barrier height decreased to only 1.7 kJ/mol at the CASSCF(7,7)+MRCI(5,7) level. The present quantum chemical calculations were performed using CASCCF(11,12)+MRCI-F12(11,12) with an augmented VTZ basis, a method which is close to a full active space, and show no barrier for approach over the ground <sup>2</sup>B<sub>1</sub> state in C<sub>2v</sub> symmetry, perpendicular to the C≡C bond (among the various approaches, the C<sub>2v</sub> interaction is the most attractive one). Furthermore, these calculations also predict a very small barrier for the first excited <sup>2</sup>B<sub>2</sub> electronic state of 0.8 kJ/mol without ZPE correction, while all the other three electronic states are strongly repulsive (see Figure 4). Considering the results obtained here, there is little doubt that the N(<sup>2</sup>D) + C<sub>2</sub>H<sub>2</sub> reaction is barrierless for at least one of the five doublet potential energy curves. Our results, using the explicitly correlated internally contracted multireference configuration interaction method with the Davidson correction (MRCI + Q) associated with complete active space self-consistent field (CASCCF) wavefunctions and a large active space, show no barrier for the N(<sup>2</sup>D) + C<sub>2</sub>H<sub>2</sub> reaction. This clearly shows the importance of the method used, as previous calculations at a lower level<sup>12, 48</sup> predicted a barrier for this process, in poor agreement with the experimental results.

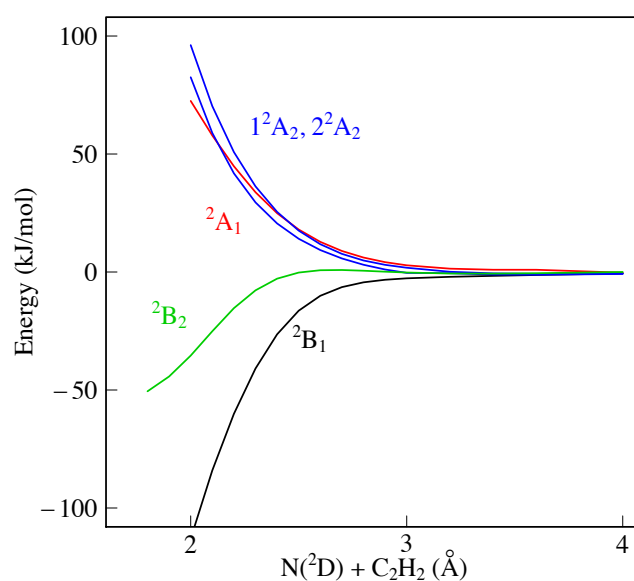


**Figure 4** Profiles of the five electronic state potential curves for the  $N(^2D) + C_2H_2$  reaction calculated at the MRCI-F12/AVTZ level of accuracy.

A realistic calculation of the rate constant would require a complete description of the first two potential surfaces while also including non-adiabatic effects at long distance. Indeed, as already demonstrated by Takayanagi et al., the use of partition functions of 0.2 (if only the first doublet surface is barrierless) or 0.4 (if the first two doublet surfaces are barrierless) might still be too small to reproduce the experimental results.<sup>12, 48</sup> Further statistical calculations should be performed on this system, by employing the new energies to examine the effect on the calculated rate constants.

To examine the influence of the present measurements on the chemistry of planetary atmospheres, we included the new rate constants for the  $N(^2D) + C_2H_2$  reaction in a photochemical model of Titan's atmosphere. We employed the 1D-model of Dobrijevic et al.<sup>56</sup> updated with the chemistry of aromatic compounds,<sup>57</sup> (see Dobrijevic et al.<sup>56</sup> for a more detailed description of the model) which treats the chemistry of neutrals and cations (we do not consider anions in this study as they play a very minor role), and the coupling between them from the lower atmosphere to the ionosphere. The neutral chemistry of nitrogen bearing molecules was already updated in previous models by these authors.<sup>22, 24, 58</sup>

Two different simulations were performed during this investigation. The first employed the currently recommended rate constants for the  $N(^2D) + C_2H_2$  reaction (where  $\alpha = 1.6 \times 10^{-10}$ ,  $\beta = 0$  and  $\gamma = 270$  in the modified Arrhenius expression  $k(T) = \alpha(T/300)^\beta e^{-\gamma/T}$ ) to yield the standard mole fraction profiles for a range of atmospheric species as a function of altitude. For the second set of simulations, the recommended rate constant values were replaced by the new ones (here we adopt a temperature independent value of  $1.1 \times 10^{-10} \text{ cm}^3 \text{ s}^{-1}$ ). In terms of the various reaction pathways, as shown in Figure 5 (adapted from Balucani et al.<sup>20</sup>), there are several possible products of the  $N(^2D) + C_2H_2$  reaction.

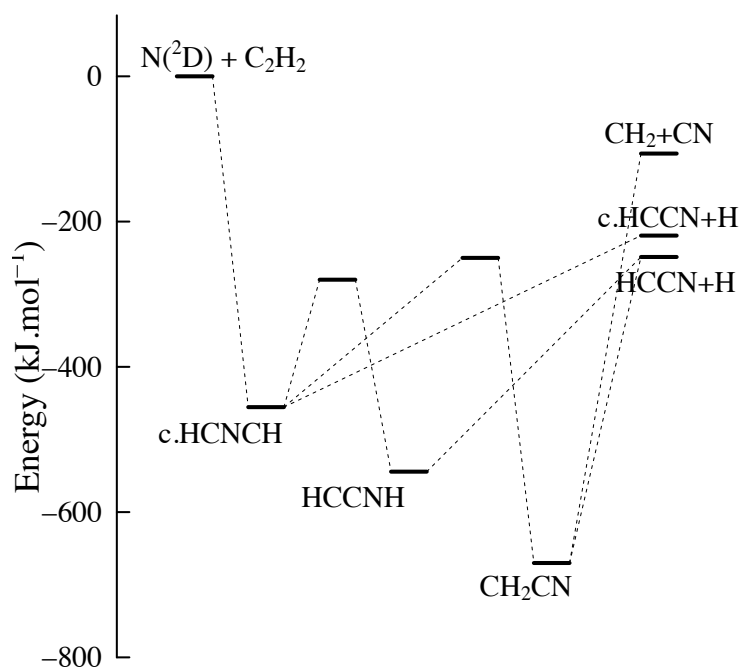


**Figure 5** Schematic energy level diagram for the  $N(^2D) + C_2H_2$  reaction (adapted from Balucani et al.<sup>20</sup>)

Despite its relatively similar energy, cyclic-HCCN is thought to be only a minor product, representing about 10% of the total from RRKM calculations by Balucani et al.<sup>20</sup> The remaining 90% of products are thought to be HCCN + H. In Titan's atmosphere, cyclic-HCCN will mainly react with hydrogen atoms leading to either linear HCCN or similar products to the  $H + HCCN$  reaction, namely  $H_2 + CCN$ .<sup>24, 58</sup> Consequently, we consider that this reaction leads to  $H + HCCN$  as the exclusive products in our model. The differences produced by the two models for various nitrogen bearing species are summarized in Table 3.

**Table 3** Difference in the mole fractions produced by the two model runs (average over the 150-1500 km range).

Species	Difference (with respect to the standard model) / %
HCCN	+136
CCN	+121
$CH_3C_3N$	+78
$C_2N_2$	+45
$CH_3CN$	-11

NH <sub>3</sub>	-9
CH <sub>2</sub> NH	-15

The new rate constants for the N(<sup>2</sup>D) + C<sub>2</sub>H<sub>2</sub> reaction make this the major loss process for N(<sup>2</sup>D) in the updated model, followed by the N(<sup>2</sup>D) + CH<sub>4</sub>, N(<sup>2</sup>D) + HCN and N(<sup>2</sup>D) + C<sub>2</sub>H<sub>4</sub> reactions.<sup>22</sup> They also induce a notable increase in the HCCN abundance, the other major HCCN source being the CH + HCN reaction.<sup>59, 60</sup> The increased production of HCCN has a significant impact on several related species. The mole fractions of CCN and NCCN increase due to increased contributions from the H + HCCN → H<sub>2</sub> + CCN<sup>24, 59</sup> and N + HCCN → H + NCCN<sup>24</sup> reactions (the increase for C<sub>2</sub>N<sub>2</sub> is smaller, as C<sub>2</sub>N<sub>2</sub> is also produced through the CN + HNC<sup>61</sup> and N(<sup>4</sup>S) + CH<sub>2</sub>CN<sup>24</sup> reactions, whereas the H + HCCN reaction is the major source of CCN radicals). The CH<sub>3</sub>C<sub>3</sub>N mole fraction also increases significantly as a result of the CCN + C<sub>2</sub>H<sub>4</sub> reaction.<sup>62</sup> The increased loss of N(<sup>2</sup>D) through the N(<sup>2</sup>D) + C<sub>2</sub>H<sub>2</sub> reaction also has an effect on the products of other competing N(<sup>2</sup>D) reactions. The simulated mole fraction of CH<sub>2</sub>NH decreases due to the lower flux of the N(<sup>2</sup>D) + CH<sub>4</sub> reaction (CH<sub>2</sub>NH is also produced through the NH + CH<sub>3</sub> reaction<sup>63</sup>). This is also the case with CH<sub>3</sub>CN, as this molecule is a product of the N(<sup>2</sup>D) + C<sub>2</sub>H<sub>4</sub> reaction<sup>17, 18, 20, 21, 64</sup> but is also produced through the N(<sup>4</sup>S) + C<sub>2</sub>H<sub>3</sub> reaction.<sup>66</sup> Similarly, the NH<sub>3</sub> mole fraction also decreases as it forms mostly from reactions of NH<sub>2</sub>, where NH<sub>2</sub> is mainly produced by NH and CH<sub>2</sub>NH reactions (NH and CH<sub>2</sub>NH are both products of the N(<sup>2</sup>D) + CH<sub>4</sub> reaction).<sup>56, 66</sup>

While the new model results are similar to those of the standard model for the majority of Titan's other atmospheric species, it will be interesting to test the effects of the new and more realistic error bars for these reactions on the mole fraction profiles of a range of atmospheric species obtained through uncertainty propagation studies. Previous uncertainty propagation studies (see Loison et al.<sup>57</sup> for example) employed uncertainty factors, for the N(<sup>2</sup>D) + C<sub>2</sub>H<sub>2</sub> reaction, deduced from previous experimental<sup>7, 12, 23</sup> and theoretical<sup>12, 48</sup> results. In light of the present experimental results, it is clear that these uncertainties were severely underestimated. It should also be noted that as the branching ratios of N(<sup>2</sup>D) reactions are mostly deduced from theoretical calculations, the values can therefore be quite approximate, illustrating the difficulty of attributing realistic uncertainties for such reactions. As further experimental studies of other important N(<sup>2</sup>D) reactions are currently underway, a more detailed uncertainty propagation study will be performed at a later date once their rate constants and associated uncertainties have been fully characterized.

## 6 Conclusions

This work reports an experimental investigation of the  $N(^2D) + C_2H_2$  reaction down to temperatures as low as 50 K, using a supersonic flow reactor.  $N(^2D)$  atoms were generated by chemical reaction during this study, while pulsed vacuum ultraviolet laser induced fluorescence was used to follow the  $N(^2D)$  kinetics directly. In parallel, electronic structure calculations were performed at a higher level than those used in previous work to better understand the experimental results. The measured rate constants were seen to be substantially larger than those obtained during the only other temperature dependent study of the  $N(^2D) + C_2H_2$  reaction, which also showed that the rate constants decreased to low temperature. In contrast, the present results show that this reaction remains rapid as the temperature falls, with a value that is approximately independent of temperature over the 50-296 K range. The present experimental results are supported by new electronic structure calculations that indicate the absence of a barrier over at least one of the potential energy surfaces connecting the reagents to products. As earlier studies determined an activation barrier for the  $N(^2D) + C_2H_2$  reaction, it is clear that the results of such calculations are highly method dependent. When the effects of the new rate constants were tested on a 1D photochemical model of Titan's atmosphere, the fractional abundances of several nitrogen bearing species such as HCCN, CCN and  $CH_3C_3N$  are seen to increase substantially, highlighting the relative importance of the  $N(^2D) + C_2H_2$  reaction on the overall photochemistry.

## Conflicts of interest

There are no conflicts to declare.

## Acknowledgements

K. M. H. and D. N. R. acknowledge support from the French program "Physique et Chimie du Milieu Interstellaire" (PCMI) of the CNRS/INSU with the INC/INP co-funded by the CEA and CNES as well as funding from the "Program National de Planétologie" (PNP) of the CNRS/INSU.

## References

1. J. Daranlot, M. Jorfi, C. Xie, A. Bergeat, M. Costes, P. Caubet, D. Xie, H. Guo, P. Honvault and K. M. Hickson, *Science*, 2011, **334**, 1538-1541.
2. J. Daranlot, U. Hincelin, A. Bergeat, M. Costes, J. C. Loison, V. Wakelam and K. M. Hickson, *Proc. Natl. Acad. Sci. U S A*, 2012, **109**, 10233-10238.

3. J. Daranlot, X. Hu, C. Xie, J.-C. Loison, P. Caubet, M. Costes, V. Wakelam, D. Xie, H. Guo and K. M. Hickson, *Phys. Chem. Chem. Phys.*, 2013, **15**, 13888-13896.
4. J.-C. Loison, X. Hu, S. Han, K. M. Hickson, H. Guo and D. Xie, *Phys. Chem. Chem. Phys.*, 2014, **16**, 14212-14219.
5. J. W. Stubbing, G. Vanuzzo, A. Moudens, J.-C. Loison and K. M. Hickson, *J. Phys. Chem. A*, 2015, **119**, 3194-3199.
6. G. Black, T. G. Slinger, G. A. St. John and R. A. Young, *J. Chem. Phys.*, 1969, **51**, 116-121.
7. B. Fell, I. V. Rivas and D. L. McFadden, *J. Phys. Chem*, 1981, **85**, 224-228.
8. H. Umemoto, N. Hachiya, E. Matsunaga, A. Suda and M. Kawasaki, *Chem. Phys. Lett.*, 1998, **296**, 203-207.
9. H. Umemoto, T. Nakae, H. Hashimoto, K. Kongo and M. Kawasaki, *J. Chem. Phys.*, 1998, **109**, 5844-5848.
10. T. Takayanagi, Y. Kurosaki, K. Sato, K. Misawa, Y. Kobayashi and S. Tsunashima, *J. Phys. Chem. A*, 1999, **103**, 250-255.
11. K. Sugawara, Y. Ishikawa and S. Sato, *Bull. Chem. Soc. Jpn.*, 1980, **53**, 3159-3164.
12. T. Takayanagi, Y. Kurosaki, K. Misawa, M. Sugiura, Y. Kobayashi, K. Sato and S. Tsunashima, *J. Phys. Chem. A*, 1998, **102**, 6251-6258.
13. H. Gao, L. Yang, Y. Pan, J. Zhou, C. Y. Ng and W. M. Jackson, *J. Chem. Phys.*, 2011, **135**, 134319.
14. P. O. Wennberg, J. G. Anderson and D. K. Weisenstein, *J. Geophys. Res-Atmos.*, 1994, **99**, 18839-18846.
15. D. Nuñez-Reyes and K. M. Hickson, *Phys. Chem. Chem. Phys.*, 2018, **20**, 17442-17447.
16. N. Balucani, F. Leonori, R. Petrucci, M. Stazi, D. Skouteris, M. Rosi and P. Casavecchia, *Faraday Discuss.*, 2010, **147**, 189-216.
17. N. Balucani, L. Cartechini, M. Alagia, P. Casavecchia and G. G. Volpi, *J. Phys. Chem. A*, 2000, **104**, 5655-5659.
18. N. Balucani, D. Skouteris, F. Leonori, R. Petrucci, M. Hamberg, W. D. Geppert, P. Casavecchia and M. Rosi, *J. Phys. Chem. A*, 2012, **116**, 10467-10479.
19. N. Balucani, A. Bergeat, L. Cartechini, G. G. Volpi, P. Casavecchia, D. Skouteris and M. Rosi, *J. Phys. Chem. A*, 2009, **113**, 11138-11152.
20. N. Balucani, M. Alagia, L. Cartechini, P. Casavecchia, G. G. Volpi, K. Sato, T. Takayanagi and Y. Kurosaki, *J. Am. Chem. Soc.*, 2000, **122**, 4443-4450.
21. S.-H. Lee, C.-H. Chin, W.-K. Chen, W.-J. Huang and C.-C. Hsieh, *Phys. Chem. Chem. Phys.*, 2011, **13**, 8515-8525.
22. D. Nuñez-Reyes, J.-C. Loison, K. M. Hickson and M. Dobrijevic, *Phys. Chem. Chem. Phys.*, 2019, **21**, 6574-6581.
23. J. T. Herron, *J. Phys. Chem. Ref. Data*, 1999, **28**, 1453-1483.
24. J. C. Loison, E. Hébrard, M. Dobrijevic, K. M. Hickson, F. Caralp, V. Hue, G. Gronoff, O. Venot and Y. Bénilan, *Icarus*, 2015, **247**, 218-247.
25. N. Daugey, P. Caubet, B. Retail, M. Costes, A. Bergeat and G. Dorthe, *Phys. Chem. Chem. Phys.*, 2005, **7**, 2921-2927.
26. N. Daugey, P. Caubet, A. Bergeat, M. Costes and K. M. Hickson, *Phys. Chem. Chem. Phys.*, 2008, **10**, 729-737.
27. J. Daranlot, A. Bergeat, F. Caralp, P. Caubet, M. Costes, W. Forst, J. C. Loison and K. M. Hickson, *ChemPhysChem*, 2010, **11**, 4002-4010.
28. R. J. Shannon, C. Cossou, J.-C. Loison, P. Caubet, N. Balucani, P. W. Seakins, V. Wakelam and K. M. Hickson, *RSC Adv.*, 2014, **4**, 26342-26353.
29. K. M. Hickson, J.-C. Loison, J. Bourgalais, M. Capron, S. D. Le Picard, F. Goulay and V. Wakelam, *Astrophys. J.*, 2015, **812**, 107.

30. K. M. Hickson, J.-C. Loison, D. Nuñez-Reyes and R. Méreau, *J. Phys. Chem. Lett.*, 2016, **7**, 3641-3646.
31. J. Bourgalais, M. Capron, R. K. A. Kailasanathan, D. Osborn, L. , K. M. Hickson, J.-C. Loison, V. Wakelam, F. Goulay and S. D. Le Picard, *Astrophys. J.*, 2015, **812**, 106.
32. K. M. Hickson, J.-C. Loison, H. Guo and Y. V. Suleimanov, *J. Phys. Chem. Lett.*, 2015, **6**, 4194-4199.
33. K. M. Hickson, J.-C. Loison, F. Lique and J. Kłos, *J. Phys. Chem. A*, 2016, **120**, 2504-2513.
34. K. M. Hickson, J.-C. Loison and V. Wakelam, *Chem. Phys. Lett.*, 2016, **659**, 70-75.
35. Q. Y. Meng, K. M. Hickson, K. J. Shao, J.-C. Loison and D. H. Zhang, *Phys. Chem. Chem. Phys.*, 2016, **18**, 29286-29292.
36. D. Nuñez-Reyes and K. M. Hickson, *J. Phys. Chem. A*, 2017, **121**, 3851-3857.
37. D. Nuñez-Reyes and K. M. Hickson, *Chem. Phys. Lett.*, 2017, **687**, 330-335.
38. D. Nuñez-Reyes and K. M. Hickson, *J. Phys. Chem. A*, 2018, **122**, 4696-4703.
39. K. M. Hickson and Y. V. Suleimanov, *Phys. Chem. Chem. Phys.*, 2017, **19**, 480-486.
40. R. Grondin, J.-C. Loison and K. M. Hickson, *J. Phys. Chem. A*, 2016, **120**, 4838-4844.
41. K. M. Hickson and Y. V. Suleimanov, *J. Phys. Chem. A*, 2017, **121**, 1916-1923.
42. D. Nuñez-Reyes, K. M. Hickson, P. Larrégaray, L. Bonnet, T. González-Lezana and Y. V. Suleimanov, *Phys. Chem. Chem. Phys.*, 2018, **20**, 4404-4414.
43. D. Nuñez-Reyes, J. Kłos, M. H. Alexander, P. J. Dagdigian and K. M. Hickson, *J. Chem. Phys.*, 2018, **148**, 124311.
44. D. Nuñez-Reyes and K. M. Hickson, *J. Phys. Chem. A*, 2018, **122**, 4002-4008.
45. T. Suzuki, Y. Shihira, T. Sato, H. Umemoto and S. Tsunashima, *J. Chem. Soc., Faraday Trans*, 1993, **89**, 995-999.
46. C. L. Lin and F. Kaufman, *J. Chem. Phys.*, 1971, **55**, 3760-3770.
47. A. Bergeat, T. Calvo, G. Dorthe and J.-C. Loison, *Chem. Phys. Lett.*, 1999, **308**, 7-12.
48. T. Takayanagi, Y. Kurosaki, K. Yokoyama, K. Sato and S. Tsunashima, *Chem. Phys. Lett.*, 1999, **312**, 503-510.
49. D. Chastaing, S. D. Le Picard, I. R. Sims and I. W. M. Smith, *Astron. Astrophys.*, 2001, **365**, 241-247.
50. D. C. Clary, E. Buonomo, I. R. Sims, I. W. M. Smith, W. D. Geppert, C. Naulin, M. Costes, L. Cartechini and P. Casavecchia, *J. Phys. Chem. A*, 2002, **106**, 5541-5552.
51. H. H. Nelson, H. Helvajian, L. Pasternack and J. R. McDonald, *Chem. Phys.*, 1982, **73**, 431-438.
52. H. Reisler, M. Mangir and C. Wittig, *Chem. Phys.*, 1980, **47**, 49-58.
53. J. Benedikt, D.J. Eijkman, W. Vandamme, S. Agarwal and M. C. M. van de Sanden, *Chem. Phys. Lett.*, 2005, **402**, 37-42.
54. H. -B. Xie, Y. -H. Ding and C. -C. Sun, *J. Comput. Chem.*, 2006, **27**, 641-660.
55. J. D. Adamson, J. D. DeSain, R. F. Curl and G. P. Glass, *J. Phys. Chem. A* 1997, **101**, 864-870.
56. M. Dobrijevic, J. C. Loison, K. M. Hickson and G. Gronoff, *Icarus*, 2016, **268**, 313-339.
57. J. C. Loison, M. Dobrijevic and K. M. Hickson, *Icarus*, 2019, **329**, 55-71.
58. E. Hébrard, M. Dobrijevic, J. C. Loison, A. Bergeat and K. M. Hickson, *Astron. Astrophys.*, 2012, **541**, A21.
59. Y. Osamura and S. Petrie, *J. Phys. Chem. A*, 2004, **108**, 3615-3622.
60. S. Zabarnick, J. W. Fleming and M. C. Lin, *Chem. Phys.*, 1991, **150**, 109-115.
61. S. Petrie and Y. Osamura, *J. Phys. Chem. A*, 2004, **108**, 3623-3631.
62. J. Wang, Y.-H. Ding and C.-C. Sun, *ChemPhysChem*, 2006, **7**, 710-722.
63. P. Redondo, F. Pauzat and Y. Ellinger, *Planet. Space Sci.*, 2006, **54**, 181-187.

- 64 K. Sato, K. Misawa, Y. Kobayashi, M. Matsui, S. Tsunashima, Y. Kurosaki and T. Takayanagi, *J. Phys. Chem.*, 1999, **103**, 8650-8656.
- 65 W. A. Payne, P. S. Monks, F. L. Nesbitt and L. J. Stief, *J. Chem. Phys.*, 1996, **104**, 9808-9815.
- 66 R. V. Yelle, V. Vuitton, P. Lavvas, S. J. Klippenstein, M. A. Smith, S. M. Horst and J. Cui, *Faraday Discuss.*, 2010, **147**, 31-49.